



Another Link in the Chain: Archaeometallurgical Investigation of an Anchor Chain from the Nineteenth Century Akko Tower Shipwreck

N. Iddan^{1,2} · D. Ashkenazi³ · S. Ariely² · D. Cvikel¹

Received: 27 September 2019 / Accepted: 5 February 2020 / Published online: 18 February 2020
© ASM International 2020

Abstract

In the 2016 excavation season of the Akko Tower shipwreck, a ferrous stud-link anchor chain and a rod, both covered with thick encrustation and concretion, were retrieved from the site. The chain links, studs, and rod were analyzed by metallurgical methods, including: radiographic testing, x-ray fluorescence, light microscopy, scanning electron microscopy with energy-dispersive spectroscopy, optical emission spectroscopy, and microhardness measurements, in order to determine their composition and microstructure. The links and the rod were made of wrought iron, while the studs were made of gray cast iron with a significant silicon content of 2 wt.%. The welding zone of the links was identified. The chain was end-welded by forge welding, and the stud was fixed mechanically. The design and manufacturing characteristics of the chain are typical of nineteenth century stud-link anchor chain, which supports the dating of the ship. It is suggested that the chain served the secondary anchor of the ship.

Keywords Cast iron · Metallography · Microstructure · Shipwreck · Stud-link · Wrought iron

Introduction

The shipwreck designated as the Akko Tower Wreck lies at the entrance of Akko harbor, Israel, 35 m north of the Tower of Flies, in 4.4 m of water. Four seasons of underwater excavations were conducted by the Leon Recanati Institute for Maritime Studies at the University of Haifa in 2012, 2013, 2015, and 2016. The study of the shipwreck suggests that it is the remains of a 25-m-long merchant brig, built during the first half of the nineteenth century in a well-established shipyard under the influence of the French shipbuilding tradition [1].

During the last underwater excavation season (2016), a segment of a ferrous chain, covered with thick encrustation and concretion, was found under the north-western section of the shipwreck. The chain was at least 5 m long, and a 2.3-m-long segment was retrieved for further study (Fig. 1). Preliminary examination of the chain exposed a ferrous rod, encased in concretion (Fig. 1a). The rod, measured after the removal of the concretion, was 56 cm long and 35 mm in diameter (Fig. 1b). The rod was well preserved, but slightly bent. The concretion was mechanically removed from the chain segment. Preliminary visual examination indicated that it was composed of 30 planar, oval ferrous links, each with a stud at its center (Fig. 2a). The major and minor axes of a typical link were 12.5 cm and 7.5 cm. The bar forming the link varied between 17 and 22 mm diameter (roughly equivalent to 11/16 and 7/8 inches), with a thickening of 2 mm at the interface with the stud. A typical stud was 3.6 cm long, 15 mm diameter at the stud center and 22 mm at the interface with the link. No manufacturer's marks or proofing stamps were detected on the links and studs.

The stud-link chain is an important element in the anchoring and mooring system of a ship. Anchor chain first appeared about 1800 [2, p. 233, 3, p. 125, 4, p. 72] as a replacement for hemp cable. The gradual transition from

✉ D. Ashkenazi
danaa@tauex.tau.ac.il; dana.ashkenazi@gmail.com

¹ Department of Maritime Civilizations and Leon Recanati Institute for Maritime Studies, University of Haifa, 3498838 Haifa, Israel

² Materials Laboratory, Israel Electric Corporation, P.O.B 10, 310001 Haifa, Israel

³ School of Mechanical Engineering, Tel Aviv University, 6997801 Ramat Aviv, Israel

Fig. 1 The chain segment retrieved from the shipwreck: (a) the as retrieved concreted chain segment (the arrow shows the concreted iron rod); and (b) general view of the iron stud-link chain and rod after removal of the concretion (Photos: A. Efremov and N. Iddan)

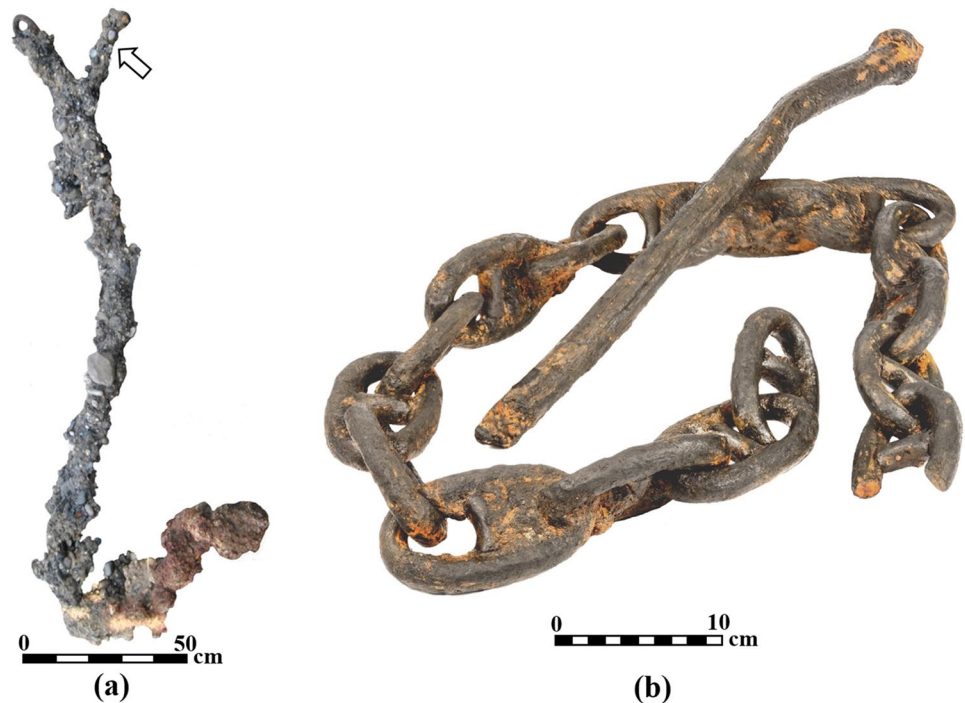


Fig. 2 The chain segment after removal of the concretion: (a) general view of the chain; and (b) the links with stud at their center



hemp to chain was one of the markers of the transition from the age of sail to the age of steam. This transition and its importance in maritime history have been thoroughly reviewed by Harland [5].

The documented use of stud-link anchor chain in the Royal Navy began about 1810, following its simultaneous development by Royal Navy Captain Samuel Brown and the industrialist Thomas Brunton. The introduction of studs (or stay-pins) in the links was intended to prevent kinking or entanglement of the anchor chain during quick release of an anchor, improving the mechanical properties of the chain link structure and preventing the plastic

deformation of the chain link under excessive stress [2, p. 233, 3, p. 125, 6, p. 51, 7, p. 112, 8, p. 461]. The size of a chain was dictated by the diameter of the iron bar from which the links were forged [2, p. 234]. The design, manufacturing process, quality control, standardization, and testing of stud-link anchor chains were extensively discussed by Admiralty and industry figures in the nineteenth century. These discussions yielded numerous textual sources devoted to the manufacture and usage of anchor chains [9, p. 100]. The use of exclusively British sources for this discussion can be justified by the fact that, at the time, the British maritime industry was the world's

leader in this field, and other countries' naval administrations largely followed British regulations [10].

Cast and wrought iron manufacturing technology underwent significant developments concurrently with the development of rigging technology and practices during the first half of the nineteenth century. These two fields of technology intersected in the anchor chain and rod retrieved from the Akko Tower shipwreck. A very brief overview of ferrous manufacturing technology is given here for the benefit of the reader less familiar with the subject.

Wrought iron objects were produced in antiquity by the 'bloomery' direct smelting technique [11–14]. In this technique, iron ore was reduced in a furnace to iron in the form of a relatively small globules, referred to as a 'bloom.' The bloom was a heterogeneous composite material, containing a large concentration of slag inclusions. Further, hot forging was essential to minimize the quantity of slag inclusions and to transform the bloom into an iron ingot appropriate for additional working processes [11, 13, 15].

In the eighteenth century, an indirect smelting method called the 'puddling' technique was developed to refine pig iron into malleable wrought iron. This process made it possible to follow the demands of the growing industry, and to increase wrought iron production capacity by replacing increasingly scarce charcoal fuel with coal and preventing contact between the metal and detrimental impurities (mainly sulfur) in the fuel [16, pp. 128–129, 146, 166]. The stirring of molten pig iron during the process exposed the metal uniformly to the elevated temperature of burning gas, reducing the iron oxide and decreasing the amount of carbon in the alloy, leading to formation of small lumps of semi-solid iron in the liquid material, which were collected and worked into larger pieces [16, pp. 128–129, 146, 166]. The typical microstructure of wrought iron objects produced by the 'puddling' technique consisted of a ferritic matrix combined with embedded elongated slag inclusions, indicating the direction of plastic deformation during the forging process [17–20]. The 'puddling' process of refining cast iron into wrought iron continued to be common until the middle of the nineteenth century [13]. The direct 'bloomery' and indirect 'puddling' iron production methods were used up to the middle of the nineteenth century, when the Bessemer process was developed and the use of wrought iron declined [15].

During the nineteenth century, the most common joining techniques for metal alloys were forge welding and riveting [16, pp. 174–175]. A satisfactory forge-welding process provided appropriate mechanical deformation (thickness reduction) to create the contact between the parts to be joined, and flux material to help clean the surfaces to be joined [11, 21]. As the deformation during the forge-welding process increases, the bond strength will increase until it reaches an optimal deformation value,

which depends on both material and process parameters [22, p. 227]. The typical forge-welding process during the nineteenth century consisted of dipping the hot workpieces in flux and continuing heating the iron parts to be joined to cherry-red color. The flux on the surfaces then fused and dissolved the iron oxide. Next, the two surfaces were positioned together and struck repeatedly [23, pp. 286–287, 24, 25]. When two wrought iron parts are forge welded, some residual oxides are entrapped along the weld [26, 27]. Nevertheless, several thermo-mechanical operations of heating and forging may result in homogenizing the wrought iron matrix and correspondingly deleting the welding line [17, 21].

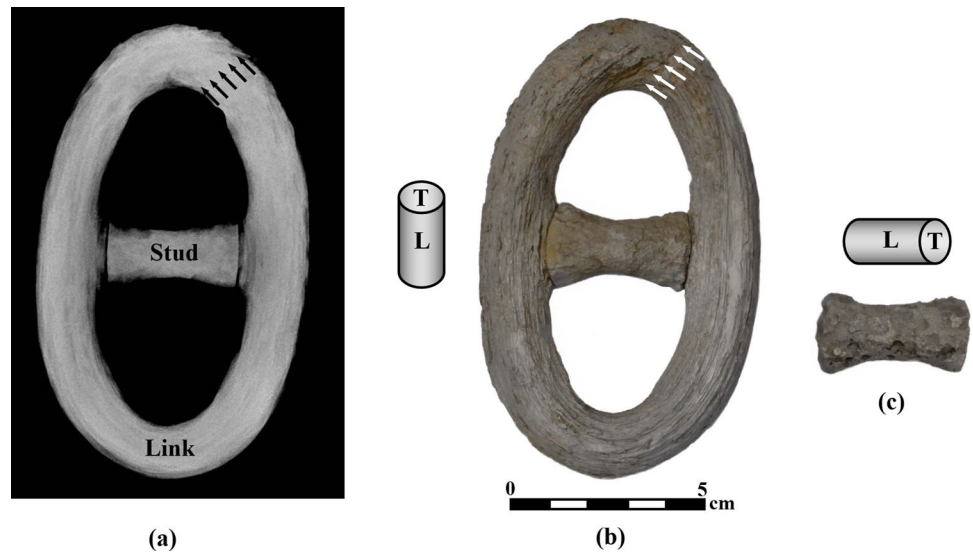
Cast iron is a group of iron alloys that contains more than 2 wt.% of carbon. The type—gray or white, and microstructure of a cast iron, depends on the composition, heat release rate during the casting process, and the cooling rate during solidification [28]. Gray cast iron, named after the color of its fracture surface, is a term that describes various cast irons whose microstructures are characterized by the content of more than 2 wt.% carbon in the form of graphite particles [29]. Increased carbon amount results in a reduction in the melting temperature of the alloy. Gray cast iron usually contains 1–3 wt.% silicon as a graphite stabilizer element that causes carbon to precipitate as dark flakes of graphite, surrounded by a ferrite and/or pearlite matrix [30, pp. 9–10, 31, p. 326].

In spite of the important role of the stud-link chain as a technological innovation in maritime history, and its interesting metallurgical features, namely the forge welding of the link and the combination of two very different ferrous materials (wrought iron and cast iron), no metallurgical study of a stud-link anchor chain from the first half of the nineteenth century has been made until now. Further understanding of the metallurgical properties of the anchor chain may provide more context for the Akko Tower shipwreck, enable the comparison between contemporary textual evidence and an example, and further the understanding of the technological state of contemporary mooring and anchoring equipment.

Experimental Methods and Tests

Radiographic testing (RT) of two links before sandblasting identified visible discontinuities and determined their state of preservation with minimum damage to the retrieved metal. After removing the concretion, three links were cut from the chain (Fig. 2b) and cleaned by sandblasting to remove the external corrosion layer (Fig. 3). The links, studs, and iron rod were analyzed by metallurgical methods, as described below:

Fig. 3 Typical chain link: (a) RT of the link covered with corrosion (before sandblasting) revealing the lack of a weld between the stud and the link; (b) the link after sandblasting showing the welding zone (white arrows); and (c) the stud after sandblasting



- (a) Visual examination of the objects identified visible discontinuities and macroscopic defects.
- (b) Chemical analysis of the link and stud bulks (after polishing) was carried out with a calibrated handheld x-ray fluorescence (XRF) instrument, equipped with a 45 kV Rh target x-ray tube. The area examined was approximately 20 mm². Light elements, including oxygen and carbon, could not be detected due to instrumental limitations.
- (c) Optical emission spectroscopy (OES) instrument determined carbon content with a detection limit of less than 0.1% [17, p. 110].
- (d) For metallographic examinations of the links, the samples were cut into longitudinal (L-CS) and transverse (T-CS) sections according to ASTM E3-11 (2011) Standard and mounted in Bakelite. The surface was ground with 80–4000 silicon carbide grit papers, polished with 1 μm aluminum oxide polishing suspension and then with 0.04 μm colloidal silica suspension. After each step, the samples were cleaned to remove contaminants. The specimens were then etched with Nital (97% alcohol, 3% HNO₃), and their microstructure was examined with a light microscope (LM).
- (e) Chemical analysis was performed using a scanning electron microscope (SEM) with an energy-dispersive spectroscope (EDS), equipped with a silicon drift detector, with an approximate error of 0.1–1%.
- (f) Vickers microhardness of the ground and polished metallographic specimens was measured with 200 gf load for 15 s.

Results

RT examination of a selected chain link, including its stud, covered with encrustation and concretion coating, indicated that it was well preserved (Fig. 3a). Such encrustation and concretion coating protects the object from accelerated corrosion and is typical of iron objects retrieved from an underwater environment after a long burial period [18, pp. 1245, 1248, 20, pp. 19–21].

Chain Links and Rod

RT examination of the chain link (Fig. 3a) showed a discontinuation of the parallel line pattern in the crown of the link, indicating the location of the weld, showing that the chain was end-welded rather than side-welded. Another finding is a clear gap between the stud and the link, indicating the absence of a metallurgical bond between the stud and the link.

Visual examination of the links after sandblasting similarly revealed a fibrous texture of parallel fine lines (Fig. 3b). The welding line was also identified visually and corresponded to the previously determined end welding point (Fig. 3b, white arrows). A macro-cross section of the link (Fig. 4a) allowed observation of the welding fusion line, the textured inclusions, and the gaps between the stud and the link.

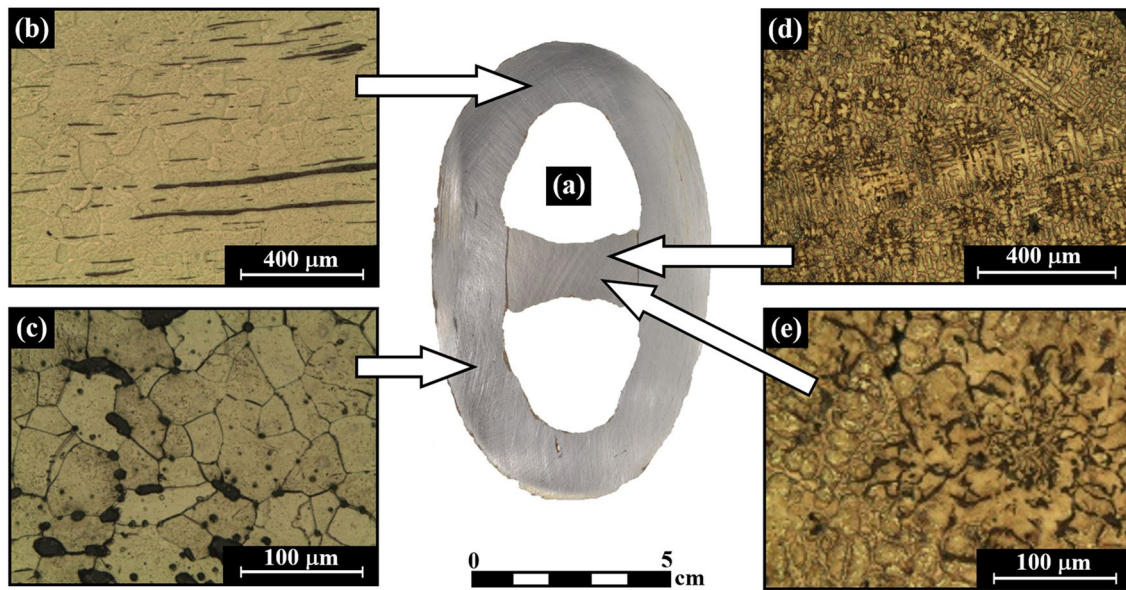


Fig. 4 Metallographic LM images of a typical chain link: (a) macroscopic view of link and stud after sandblasting; (b) general microscopic view of the link, showing preferentially oriented slag inclusions (dark areas), surrounded by iron ferrite matrix (L-CS, before

etching); (c) slag inclusions (dark areas) surrounded by iron ferrite grains (T-CS, etched); (d) general microscopic view of the stud, showing an as-cast dendritic structure (L-CS); and (e) graphite flakes (dark areas), which are typical of gray cast iron (T-CS)

Cross sections of the iron links (Fig. 4a–c) and rod (Fig. 5) were examined by using a LM. The material of the link and rod was determined to be wrought iron (Figs. 4b, c, 5, 6). The microstructure of the link material (between the ends of the link, away from the welded area) can be characterized as an equiaxial grain ferritic matrix with an extensive network of dark, heavily textured, parallel, elongated slag inclusions (Fig. 6), and a similar microstructure was identified in the rod material (Fig. 5). The absence of pearlite in the microstructure of the links and rod indicated a very low carbon content, with the combination of highly textured preferentially oriented inclusions (Fig. 6a, L-CS) and equiaxial iron grains (Figs. 5a, b, 6b) typical of wrought iron manufactured by the ‘puddling’ process, and shaped by hot forging [17, pp. 109, 114].

Based on XRF analysis, the composition of the link material was mostly iron, with the presence of 0.3 ± 0.2 wt.% Si and 0.2 ± 0.2 wt.% P (ten representative areas of the link were examined, each about 20 mm^2 in area). Similar XRF results were also observed in the rod (99.6 wt.% Fe and 0.4 wt.% Si). Based on the OES analysis results, the carbon content was 0.0648 ± 0.0003 wt.% C for the link, typical of ferritic iron.

The microstructure of the links was further studied by SEM in conjunction with compositional analysis and mapping using EDS. Single-phase, two-phase, and three-phase oxide inclusions were observed. A typical element map of the link material revealed a relatively homogeneous ferritic matrix, with a network of elongated multi-phased oxide

inclusions, containing mostly Fe, Si, P, Mn, and Ca (Fig. 7). An elemental analysis of a representative area, containing a typical concentration of slag (between the ends of the link, away from the weld), is presented in Table 1. The spot elemental compositions of the ferrite matrix, slag inclusions, and the two phases within the slag inclusion are also presented (Table 1).

Microhardness testing of the link and the rod revealed average hardness of 152.4 ± 3.3 HV and 156.4 ± 4.3 HV, respectively, for the ferrite matrix, typical of a wrought iron object [17, p. 122]. Since the carbon concentration was very low, the measured microhardness values are related to plastic deformation [17, p. 122]. The microhardness values of the inclusions varied greatly and averaged 369.6 ± 115.9 HV. This heterogeneous result can be attributed to cracking and the inconsistent integrity of the inclusions. For comparison, the average microhardness of the wüstite–glassy slag inclusion measured in the wrought iron deadeyes retrieved from the Akko Tower shipwreck was between 376 ± 21 (L-CS) and 414 ± 26 HV (T-CS) [18, pp. 1251, 1253], which suggests that the links and deadeyes were manufactured using a similar technology.

The weld area was first identified by radiography (Fig. 3a) and surface visual examination (Fig. 3b). The polished and etched metallographic sample of the weld area was further examined at the microscopic scale, revealing a discontinuation of the elongated inclusion texture. The sequence of non-elongated inclusions and long crevices (over 1 mm) hinted at the possible location of the

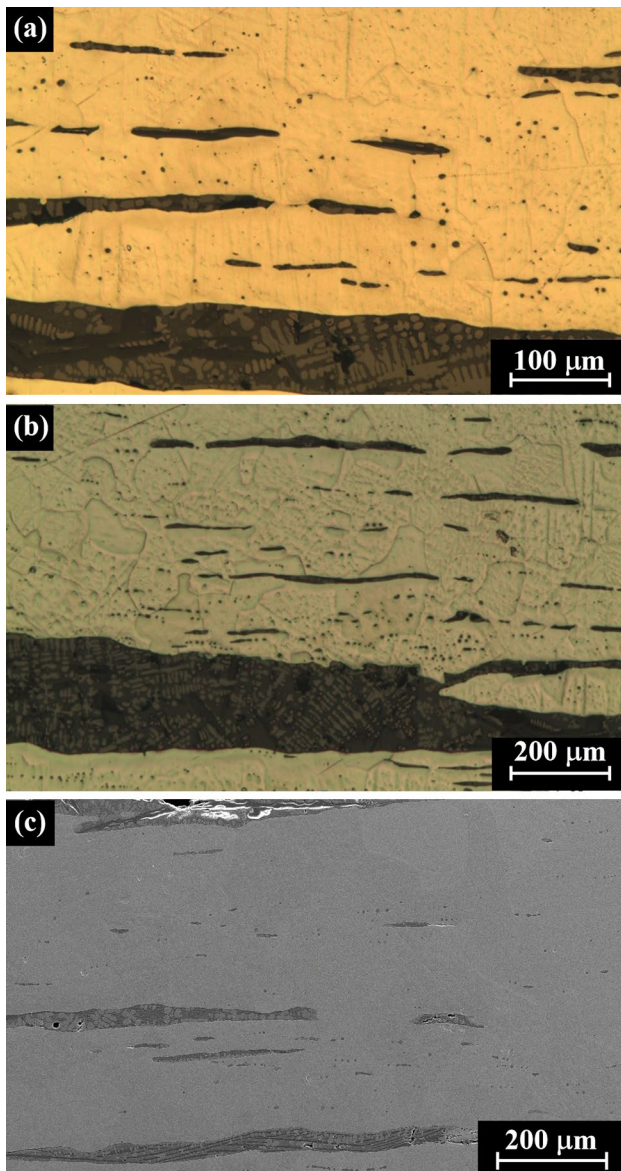


Fig. 5 Metallographic images of the wrought iron rod: (a) and (b) preferentially oriented slag inclusions (dark parallel areas) surrounded by iron ferrite matrix of equiaxed grains (L-CS, LM, etched, LM); and (c) preferentially oriented slag inclusions surrounded by iron ferrite matrix (before etching, SEM)

fusion line (Fig. 8a). The shape of the slag inclusions at the forge-welding zone was different from the elongated slag inclusions dispersed throughout the bulk of the link material (Fig. 8b), as previously observed in the iron-bound deadeyes retrieved from the Akko Tower shipwreck [17, p. 122]. However, spot chemical analysis of the inclusions associated with the weld fusion line did not yield results fundamentally different from the composition of the elongated slag inclusions away from the weld (Table 1).

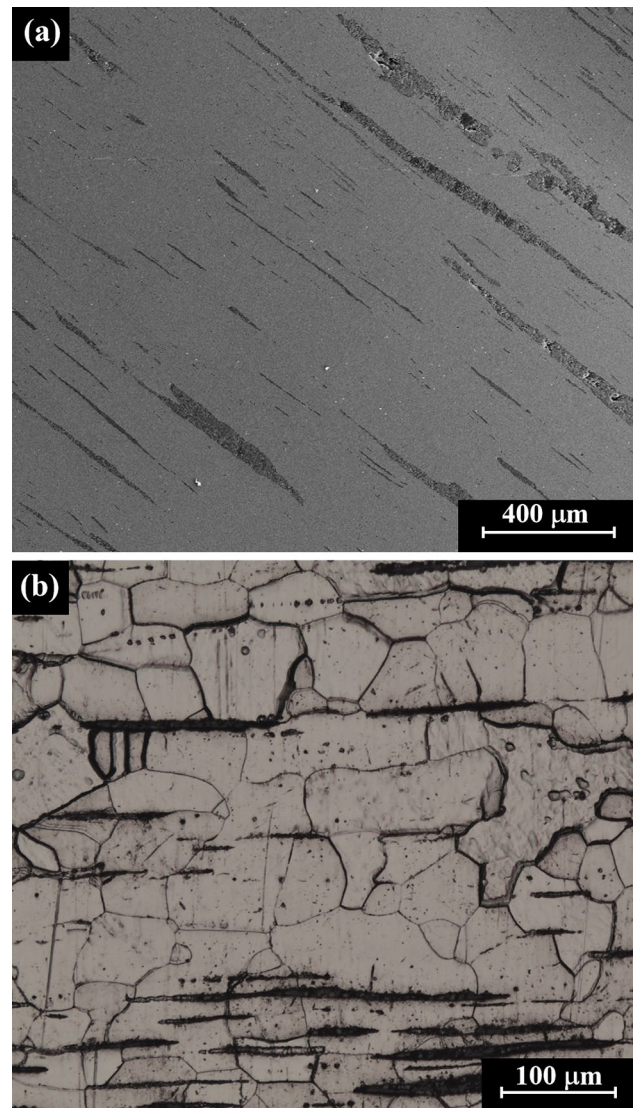


Fig. 6 Metallographic images of the wrought iron link far from the weld: (a) preferentially oriented slag inclusions (dark parallel areas) surrounded by iron ferrite matrix (L-CS, far from the welding zone, before etching, SEM); and (b) preferentially oriented slag inclusions and equiaxed ferrite grains (with grain size 20–100 μm , etched, LM)

Stud

As noted earlier, RT of the selected chain link revealed a clear gap at the interface between the stud and the link, suggesting that the stud was not welded to the link. The sandblasting process exposed the external surface of the studs, and extensive porosity was observed (Fig. 3c).

Cross sections of the iron stud (Fig. 4a) were examined by LM. The material of the stud was identified as gray cast iron (Fig. 4d–e and Fig. 9). The microstructure of the stud material, as observed by LM and SEM observations, was heterogeneous, with a dendritic structure (Fig. 9a) that included areas of ferrite, perlite, graphite flakes (Fig. 4d–e).

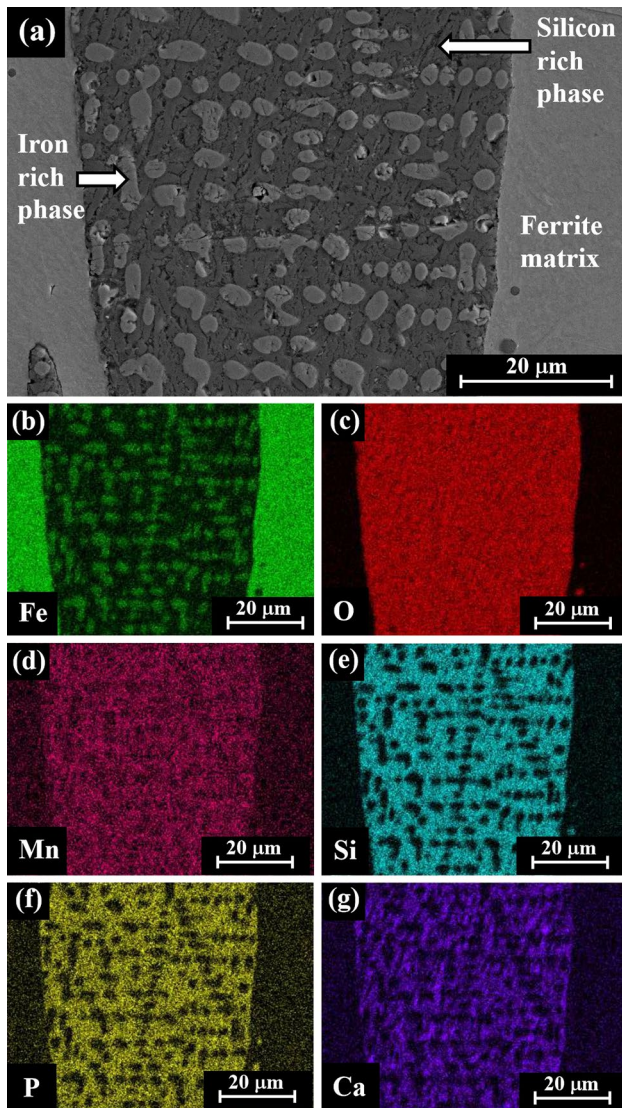


Fig. 7 Elemental SEM–EDS analysis (bright dots) of the wrought iron link, area of typical slag inclusions within the ferrite matrix (L-CS, far from the welding zone): (a) general view of the examined area; (b) iron; (c) oxygen; (d) manganese; (e) silicon; (f) phosphorus; and (g) calcium

Interdendritic porosity cast defects (Fig. 9b), manganese (II) sulfide (MnS) (Fig. 10), and steadite—iron phosphide (Fe_3P , Fig. 10c, white arrow), were also detected.

Based on XRF analysis of eight typical areas of the stud (each about 20 mm^2), the metal consisted mainly of iron, with the presence of $0.2 \pm 0.1 \text{ wt.}\%$ Mn, $1.9 \pm 0.4 \text{ wt.}\%$ Si, $0.4 \pm 0.1 \text{ wt.}\%$ P, $0.2 \pm 0.1 \text{ wt.}\%$ S, and $0.1 \pm 0.1 \text{ wt.}\%$ Ti. SEM–EDS compositional analysis and mapping of the stud are presented in Table 2 and Fig. 11. The mapping revealed the presence of Fe, C, Mg, Si, P, and S (Fig. 11). The carbon content in the stud material, according to the OES analysis, was $1.9333 \pm 0.0455 \text{ wt.}\%$ C.

The stud showed an average microhardness of $411.7 \pm 49.8 \text{ HV}$. For comparison, the microhardness of the gray cast iron chain link from the nineteenth century Dor 2002/2 shipwreck was between $317 \pm 26 \text{ HV}$ (P-CS) and $324 \pm 29 \text{ HV}$ (P-CS) [20]. The microhardness values of the stud suggest that it was chosen to withstand compression stresses. This also supports the RT results showing that the stud was not welded to the link.

Discussion

The state of development of technologies over time, combined with the use of scientific testing methods, can serve as valuable tools to distinguish between manufacturing technologies, and may contribute to the dating of metal objects retrieved from shipwreck [20, p. 25]. The metallurgical approach used in this study contributed to the understanding of the anchor chain manufacturing. The compositional analysis of the link and the stud material was supplemented with OES in order to determine their carbon content. Based on the OES analysis, the link was made of wrought iron containing about $0.1 \text{ wt.}\%$ C, typical of ferritic iron; and the stud was made of cast iron with about $2 \text{ wt.}\%$ C.

Following the compositional analysis, the link material was mostly composed of iron, with the presence of $0.3 \text{ wt.}\%$ Si and $0.2 \text{ wt.}\%$ P, where silicon and phosphorus are common elements in wrought iron slag inclusions [17, 32].

Table 1 Area and spot SEM–EDS chemical analysis of the link (wt.%)

Measured area	Composition (wt.%)											
	Fe	O	Si	Mn	P	Ca	Mg	S	Ti	Al	K	V
Wrought iron matrix with embedded inclusion particles (Fig. 6a, area scan)	95.6	2.9	0.5	0.4	0.3	0.2	0.1
Typical ferrite matrix (Fig. 7a, area scan)	99.5	...	0.1	0.2	0.2
Typical two-phase slag inclusion (Fig. 7a, area scan)	49.9	34.1	4.8	3.9	2.5	2.4	0.9	0.6	0.1	0.6	0.1	0.1
Iron-rich oxide phase in the slag (Fig. 7a, spot scan)	56.3	41.8	0.1	1.1	...	0.1	0.2	...	0.1	0.2	...	0.1
Silicon-rich oxide phase in the slag (Fig. 6a, spot scan)	43.4	36.9	7.2	3.9	3.3	2.6	1.1	0.8	...	0.6	0.2	...
Slag in the weld area (Fig. 8, area scan)	52.0	32.8	4.6	3.8	2.4	2.2	1.0	0.6	0.1	0.5

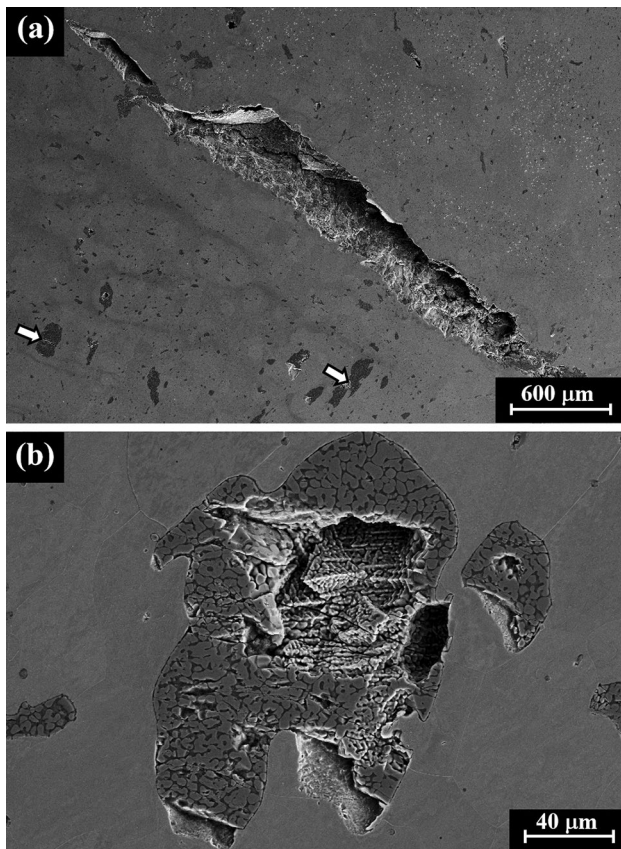


Fig. 8 Metallographic SEM image of wrought iron link microstructure: (a) large (over 1 mm) micro-fissure (white arrows) in the hypothesized weld area; and (b) a typical slag inclusion in the hypothesized weld area

Since Si does not reduce in either of the direct and indirect smelting methods, its presence represents the slag inclusion distribution in the link's wrought iron matrix [15, 17, 18]. The link and rod material was made from relatively pure ferritic iron, rich in slag inclusions, such as single-phase fayalite (Fe_2SiO_4), two-phase glass-wüstite inclusions, and three-phase glass-wüstite-fayalite, typical of wrought iron objects [17, p. 110]. However, further analyses of the inclusions, such as XRD, EBSD, TEM, are needed in order to study their phases.

Based on the homogeneous microstructure of the link and rod, they were wrought iron products, produced by the 'puddling' technique of refining pig iron into malleable wrought iron [15, 17–20]. The equiaxed iron ferrite grains in the rod (Fig. 5) and link (Fig. 6) material, combined with preferentially oriented slag inclusions, indicate that both objects were shaped by a hot-forging process, where the elongated inclusions show the direction of plastic deformation during forging. The average microhardness of the link's material (152.4 ± 3.3 HV) was typical of a ferritic wrought iron object that included small inclusions distributed relatively

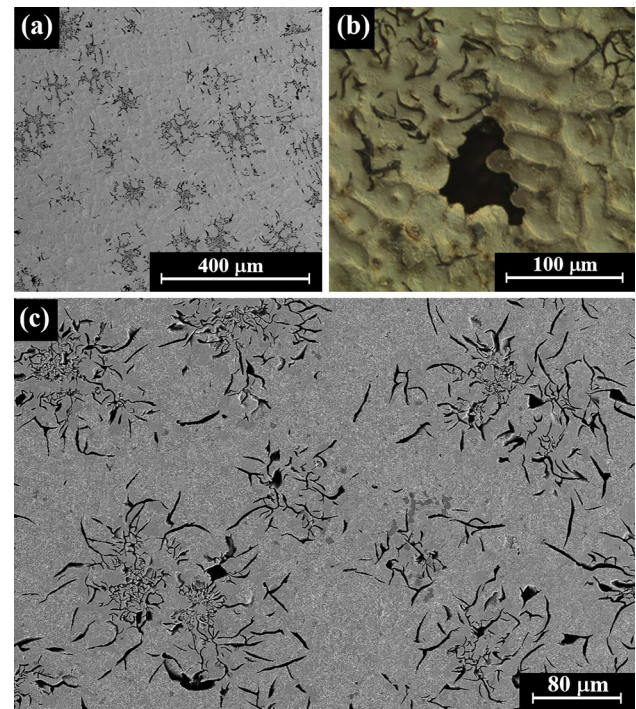


Fig. 9 Metallographic LM and SEM images of the cast stud: (a) dendritic morphology with dark graphite rosettes (assembly of dark graphite needles); (b) interdendritic porosity; and (c) ferrite and pearlite microstructure with dark graphite needles

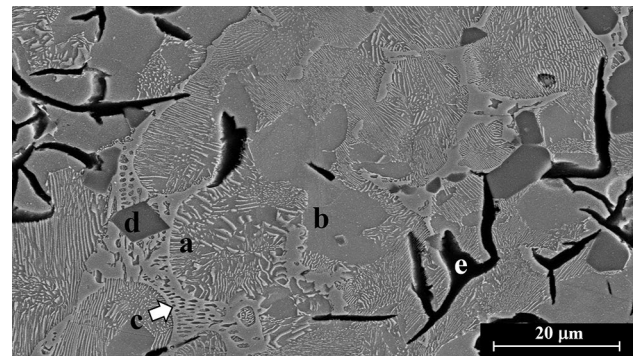


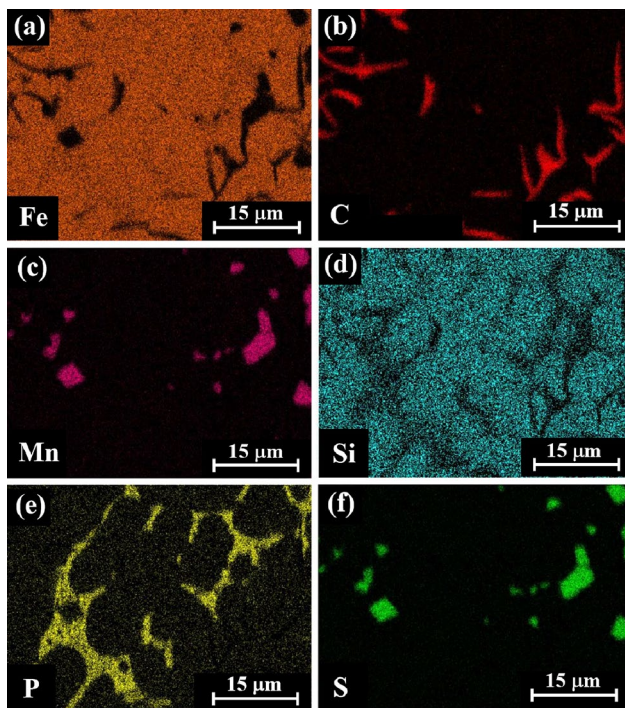
Fig. 10 Metallographic SEM image of the cast stud: (a) pearlite microstructure; (b) ferrite phase; (c) steadite iron phosphide; (d) MnS; and (e) graphite flakes

homogeneously through the ferrite matrix [17, p. 122, 20, p. 26].

According to the compositional analysis, the stud's metal consisted mainly of iron, with 1.9 wt.% Si and 0.2 wt.% Mn. The manganese may have been added deliberately in order to reduce gas porosity [14, 33, p. 2523]. The presence of 1.9 wt.% silicon, which serves as a graphite stabilizer element, was typical of gray cast iron [30, pp. 9–10, 31, p. 326]. The metallographic LM and SEM observation of the stud

Table 2 Area and spot SEM–EDS chemical analysis of the stud (wt.%)

Measured area	Composition (wt.%)						
	Fe	Si	Mn	P	S	Ti	V
Cast iron with ferrite and pearlite microstructure and embedded graphite rosettes (Fig. 9, area scan)	94.4	2.0	1.3	2.0	0.1	0.1	0.1
Typical pearlite microstructure (Fig. 10a, spot scan)	96.1	2.7	0.9	0.3
Steadite island (iron phosphide, Fig. 10c, spot scan)	83.4	0.3	2.0	13.9	...	0.1	0.3
MnS (Fig. 10d, spot scan)	2.4	...	59.3	0.1	37.9	0.2	0.1

**Fig. 11** Elemental SEM–EDS analysis (bright dots) of the cast stud: (a) iron; (b) carbon; (c) manganese; (d) silicon, (e) phosphorus; and (g) sulfur

revealed gray cast iron with a fairly uniform distribution of graphite flakes (Fig. 9). The average microhardness of the stud's material (152.4 ± 3.3 HV) was typical of gray cast iron [33, p. 2525].

In the first half of the nineteenth century, the *chaîne opératoire* of stud-link chain manufacturing comprised: procurement of rolled wrought iron bar of the appropriate diameter, cutting the bar into link-length pieces, bending the pieces to a U-shape and scarfing their edges, forge welding the link, and fixing the stud in the link [34]. The wrought iron used in the chain industry was produced by ‘puddling,’ shingling (to remove slag), and rolling cast iron. The resultant material was a very low carbon iron matrix with a network of elongated, mostly silicon dioxide, inclusions. Because anchor chains were frequently tested, higher quality wrought iron was usually used for their manufacture [35].

While the chain link itself was made of ductile wrought iron, the stud was made of brittle cast iron. This difference in material selection was the result of the different requirements for the two components [9, p. 100]. The characteristics of the link material examined are consistent with other contemporary rolled wrought iron items [17, 18, 20, 36]. These characteristics include the typical wrought iron structure of a low carbon iron matrix and a network of elongated inclusions with a high silicon oxide content [36]. Wrought iron was chosen for use in anchor chain links because of its weldability, plasticity, and impact resistance [9, p. 19, 37, p. 170].

The ends of the cast iron studs were recessed to make a tight fit with the link [9, p. 101] and were not welded to the links, but rather fixed in place by hammering or using a hydraulic press [36]. In the link examined, a non-welded interface between the link and the stud and recessed ends in the stud were indeed identified using radiography and visual examination at the macro-cross section. The stud material was determined to be gray cast iron with a rather high phosphorus content. This can be related to a lower quality raw material, such as cold blast coke pig iron [16, p. 126] used for the studs. Cast iron was chosen for this application for its compressive strength and low cost [9, p. 100].

The failure of cable chains was of grave concern in the transition from hemp to chain [4, p. 74, 8]. Testing machinery and procedures were developed together with the transition process [38]. According to Royal Navy and Lloyd's regulations, each cable chain required testing and certification. In 1845, a Royal Navy inquiry into causes of failure, headed by a prominent engineer of the time, James Nasmyth, determined that in 80 out of 100 tests, the cause of failure was the weld [39, pp. 268, 418]. Nasmyth identified the presence of oxides along the weld fusion line as the reason for the weakness. These oxides accumulated on the scarf bevels during its intense heating just prior to forge welding. Nasmyth suggested an improvement to the welding practice, whereby the scarfs would be convex to squeeze the oxide out of the fusion interface during hammering, rather than being trapped in it [39, pp. 268, 418]. The presence of discontinuities, such as pores and misaligned inclusions, in the weld area of the link, supports Nasmyth's concerns and indicates that this issue was

indeed problematic and difficult to tackle. However, the overall weld quality in the links appears to be satisfactory, and there are few discontinuities.

The size of a chain cable is measured by the diameter of the link [3, p. 125, 7, p. 112]. Tables relating to the dimensions of chains, weight of anchors, and tonnage of ships were published by Pering in 1819 and by Lloyd's in 1864. The size of the links (3/4–7/8 inch) roughly corresponds to a bower anchor of 300–400 kg (probably including the stock), and a ship of 60–100 tons according to Pering [4, p. 98], and to a bower anchor of up to 200 kg (excluding the stock), and a ship of 75–100 tons, according to the Lloyd's table cited by Gladstone [8, p. 462]. Based on both sources, one would expect the ship to have two bower anchors of between 200 and 400 kg. However, this does not match previous investigations of the ship, which suggested a larger vessel of 160–200 tons [1, p. 420, 18, p. 1256]. Nevertheless, assuming the larger size is the correct reconstruction, this discrepancy could be explained in one of two ways: the first is that the ship was not rated as A1 or equivalent (the highest class according to Lloyd's) in terms of its construction; and the other is that the chain studied here served the secondary anchor rather than the main bower.

Based on the composition, microstructure, and manufacturing technology of the stud-link anchor chain, it is proposed that it was manufactured about the middle of the nineteenth century. This dating agrees well with the dating of the ship [1, pp. 418–419]. The high quality of the link material (based on its chemical homogeneity and the texture of the slag inclusions), the stud material (considering the general lack of cracks and pores), and the high quality of the weld (based on the limited amount of discontinuities) are as expected for anchor chains, considering that both the Royal Navy and Lloyd's required a testing certificate for each anchor chain they procured. Previously investigated ferrous finds from the Akko Tower shipwreck included iron-bound deadeyes with non-studded chains and a bolt [18]. These artifacts were determined to be uniformly manufactured of wrought iron with homogeneous preferentially oriented slag inclusions. The deadeyes and their non-studded chain links were forge welded. These welds were different in style from the forge welds of the stud-link anchor chain. The forge weld of the non-studded chain was a crown weld along about half the chain link diameter, while the welds studied here were much shorter, about one tenth the link diameter, which is more consistent with the contemporary literature regarding the manufacture of stud-link anchor chains.

The exact function of the rod remains a puzzle. It was indeed found concreted with the chain, although this fact cannot definitely link the two finds. One possibility was that the rod was a fractured anchor stock; however, no sign of a 'keep pin' or other method of securing the proposed stock in place was located on the rod. No signs of any other

recognizable interfacing 'tool-marks' were identified on the rod; hence the difficulty in determining its function.

Conclusions

The links of the anchor chain from the Akko Tower shipwreck were made of wrought iron manufactured by the 'puddling' process and plastically deformed to the final shape. The links were joined by forge welding at their crowns (end-welded). The studs, fixed mechanically (rather than welded) at the center of the links, were made of gray cast iron. The contemporary textual references to the subject of anchor chains support the conclusion that the design and manufacturing characteristics of the chain are consistent with a mid-nineteenth century manufacturing process and that it perhaps served for the secondary anchor rather than the bower.

Acknowledgements

The underwater excavations (IAA excavation permits G-23/2012, G-78/2013, G-16/2015 and G-25/2016) and research of the Akko Tower Wreck were supported by the Israel Science Foundation (Grant No. 447/12), the Honor Frost Foundation, and the Rector and Research Authority of the University of Haifa, to whom the authors are grateful. The authors are grateful to J. B. Tresman for the English editing.

References

1. D. Cvikel, The 19th-Century Akko Tower Wreck, Israel: a summary of the first two excavation seasons. *Int. J. Naut. Archaeol.* **45**(2), 406–422 (2016)
2. J.H. Harland, *Seamanship in the Age of Sail: An Account of the Shiphandling of the Sailing Man-of-War 1600–1860, Based on Contemporary Sources* (Conway, London, 1985)
3. P. Kemp, *Oxford Companion to Ships and the Sea* (Oxford University Press, Oxford, 1976)
4. R.A. Pering, *Treatise on the Anchor* (Congdon & Hearle, London, 1819)
5. J.H. Harland, The transition from hemp to chain cable: Innovations and innovators. *Mar. Mirror* **99**(1), 72–85 (2013)
6. L.A. Beardslee, *Beardslee on Wrought-Iron and Chain-Cables: Experiments on the Strength of Wrought-Iron and of Chain-Cables* (Wiley, NY, 1879)
7. C.H. Brown, *Nicholls's Seamanship and Nautical Knowledge for Second Mates', Mates' and Masters' Examinations* (Brown Son and Ferguson, Glasgow, 1961)
8. T.M. Gladstone, Anchors and cables: their history, varieties, and properties. *J. Soc. Arts* **13**, 459–463 (1865)
9. R. Moss, *Chain and Anchor Making in the Black Country* (History Press, Gloucestershire, 2013)
10. F.A. Paget, On the testing of chain cables. *J. Soc. Arts* **12**, 403–414 (1864)

11. E. Blakelock, M. Martinon-Torres, H.A. Veldhuijzen, T. Young, Slag inclusions in iron objects and the quest for provenance: an experiment and a case study. *J. Archaeol. Sci.* **36**(8), 1745–1757 (2009)
12. M. Cavallini, Thermodynamics applied to iron smelting techniques. *Appl. Phys. A* **113**(4), 1049–1053 (2013)
13. J.L. Coze, Purification of iron and steels: a continuous effort from 2000 BC to AD 2000. *Mater. Trans.* **41**(1), 219–232 (2000)
14. M.L. Wayman, Archaeometallurgical contributions to a better understanding of the past. *Mater. Charact.* **45**(4), 259–267 (2000)
15. V.F. Buchwald, H. Wivel, Slag analysis as a method for the characterization and provenancing of ancient iron objects. *Mater. Charact.* **40**(2), 73–96 (1998)
16. R.F. Tylecote, *A History of Metallurgy*, 2nd edn. (The Metals Society, London, 1992)
17. I. Voiculescu, V. Geantă, A. Stern, D. Ashkenazi, M. Cohen, D. Cvikel, Iron-bound deadeyes from the nineteenth-century Akko Tower wreck, Israel: Metallurgical investigation of the manufacturing technology. *Metall. Microstruct. Anal.* **6**(2), 106–125 (2017)
18. M. Cohen, D. Ashkenazi, A. Stern, Y. Kahanov, D. Cvikel, Iron artefacts from the Akko Tower Wreck, Israel, and their contribution to the ship's characterization. *Archaeol. Anthropol. Sci.* **9**, 1243–1257 (2017)
19. D. Cvikel, D. Ashkenazi, A. Stern, Y. Kahanov, Characterization of a 12-pdr wrought-iron cannonball from the Akko 1 shipwreck. *Mater. Charact.* **83**, 198–211 (2013)
20. D. Cvikel, D. Ashkenazi, The Dor 2002/2 shipwreck, Israel: characterization of surviving ironwork. *Metall. Microstruct. Anal.* **5**(1), 16–27 (2016)
21. D. Ashkenazi, D. Cvikel, A. Stern, A. Pasternak, O. Barkai, A. Aronson, K. Kahanov, Archaeometallurgical investigation of joining processes of metal objects from shipwrecks: three test cases. *Metallogr. Microstruct. Anal.* **3**(5), 349–362 (2014)
22. S. Mahabunphachai, M. Koc, J. Ni, Characterization of pressure welding process of thin sheet metals in cold and warm temperature conditions, in *ASME 2007 International Manufacturing Science and Engineering Conference* (American Society of Mechanical Engineers, Atlanta, 2007), pp. 227–233
23. T. Lienert, T. Siewert, S. Babu, V. Acoff (eds.), *Welding Fundamentals and Processes*, *ASM Handbook*, vol. 6A (ASM International, Novelt, 2011)
24. H.A. Mohamed, J. Washburn, Mechanisms of solid state pressure welding. *Weld. J. Res. Suppl.* **54**, 302s–310s (1975)
25. A. Stern, D. Ashkenazi, D. Cvikel, B. Rosen, E. Galili, Archeometallurgical and technical characterization of 7th century AD iron fishing-spear and fire basket found in the Dor lagoon, Israel. *J. Archaeol. Sci. Rep.* **3**, 132–143 (2015)
26. A. Aronson, D. Ashkenazi, O. Barkai, Y. Kahanov, Archaeometallurgical investigation of the iron anchor from the Tantura F shipwreck. *Mater. Charact.* **78**, 108–120 (2013)
27. N.C. Ciarlo, H. De Rosa, D. Elkin, H. Svoboda, C. Vázquez, D. Vainstub, L. Diaz Perdiguero, Examination of an 18th century english anchor from Puerto Deseado (Santa Cruz Province, Argentina). *Hist. Metall.* **45**(1), 71–79 (2011)
28. R. Menon, T. McKay, Welding of cast irons and steels, in *ASM Metals Handbook Vol 15: Casting*, ed. by H.J. Frissell (ASM International, Novelt, 1996), pp. 12–54
29. M. Goodway, History of casting, in *ASM Metals Handbook Vol. 15: Casting*, ed. by H.J. Frissell (ASM International, Novelt, 1996), pp. 12–54
30. J.S. Park, M.E. Hall, The use of white cast iron in ancient Korea. *Inst. Archaeol. Stud.* **25**, 9–13 (2005)
31. W. Xu, M. Ferry, Y. Wang, Influence of alloying elements on as-cast microstructure and strength of gray iron. *Mater. Sci. Eng. A* **390**, 326–333 (2005)
32. R.E.M. Hedges, C.J. Salter, Source determination of iron currency bars through analysis of the slag inclusions. *Archaeometry* **21**(2), 161–175 (1979)
33. E.D. Mentovich, D.S. Schreiber, Y. Goren, Y. Kahanov, H. Goren, D. Cvikel, D. Ashkenazi, New insights regarding the Akko 1 shipwreck: a metallurgic and petrographic investigation of the cannonballs. *J. Archaeol. Sci.* **37**(10), 2520–2528 (2010)
34. A. Ure, *Dictionary of Arts, Manufactures, and Mines; Containing a Clear Exposition of their Principles and Practice* (D. Appleton and Co., New York, 1853)
35. P. Belford, Extra special best best: Black Country iron puddling and wrought iron manufacturing in the nineteenth Century. *Hist Metall* **38**(1), 47–59 (2004)
36. L.E. Samuels, Australia's contribution to archaeometallurgy. *Mater. Charact.* **29**, 69–109 (1992)
37. D. Ashkenazi, E. Mentovich, D. Cvikel, O. Barkai, A. Aronson, Y. Kahanov, Archaeometallurgical investigation of iron artifacts from shipwrecks—a review, in *Archaeology, New Approaches in Theory and Techniques*, ed. by I. Ollich-Castanyer (InTech, Rijeka, 2012), pp. 169–186
38. C.E. Turner, The early nineteenth-century chain testing machines. *Int. J. Hist. Eng. Tech.* **82**(2), 233–261 (2012)
39. J. Nasmyth, S. Smiles, *James Nasmyth Engineer: An Autobiography* (John Murray, London, 1883)

Publisher's Note Springer Nature remains neutral with regard to jurisdictional claims in published maps and institutional affiliations.